crystals

MDPI

Article

$LiNbO_3:Ho^{3+}$ Crystal as a Material for Radiation-Balanced Lasing in the 640–670 nm Region

Gagik Demirkhanyan [1], Narine Babajanyan [1], Frida Voskanyan [1], Ninel Kokanyan [2], Marco Bazzan [3] and Edvard Kokanyan [1,*]

[1] Department of Physics and it's Teaching Methods, Armenian State Pedagogical University after Kh. Abovyan, Yerevan 0010, Armenia
[2] Chaire Photonique, Laboratoire Matériaux Optiques Photonique et Systèmes (LMOPS), CentraleSupélec, F-57070 Metz, France
[3] Dipartimento di Fisica e Astronomia, Università di Padova, 35131 Padova, Italy
* Correspondence: edvardkokanyan@gmail.com

Abstract: Holmium-doped congruent-composition lithium niobate ($LiNbO_3$:Ho, LN:Ho) crystals were grown by the Czochralski method. The absorption of the LN:1at% Ho^{3+} crystal was recorded at room temperature. On the basis of the analysis of emission and absorption spectra of the LN:1at% Ho^{3+} crystal, the possibilities of obtaining, at room temperature, radiation-balanced (RB) lasing in the region of 640–670 nm wavelengths corresponding to the inter-Stark transitions of manifolds $^5F_5$ and $^5I_8$ was theoretically investigated. The RB lasing parameters were calculated and the optimal pump and laser wavelengths were determined: $\lambda_{OP} = 652.1$ nm, $\lambda_{OL} = 653.6$ nm. The values for the RB lasing efficiency and radiation amplification in the considered wavelength region were obtained: $F_{eff} = 3.23 \times 10^{-22}$cm^2, $F_{gain} = 6.08 \times 10^{-22}$ cm^2.

Keywords: lithium niobate crystal; absorption; rare-earth ions; radiation balanced laser

Citation: Demirkhanyan, G.; Babajanyan, N.; Voskanyan, F.; Kokanyan, N.; Bazzan, M.; Kokanyan, E. $LiNbO_3:Ho^{3+}$ Crystal as a Material for Radiation-Balanced Lasing in the 640–670 nm Region. *Crystals* **2024**, *14*, 760. https://doi.org/10.3390/cryst14090760

Academic Editor: Yuui Yokota

Received: 18 July 2024
Revised: 1 August 2024
Accepted: 8 August 2024
Published: 26 August 2024

1. Introduction

The possibility of creating a self-cooling solid-state laser (radiation- balanced laser) based on doped rare-earth (RE) ions was first proposed in [1]. The idea of a radiation-balanced (RB) laser operation is based on the possibility of full (or partial) compensation of heat generated as a result of pumping and stimulated emission processes by the cooling of anti-stokes fluorescence (ASF) in the active medium. The mechanism of optical self-cooling is quite simple: by absorbing a photon, the atom briefly leaves the state of thermal equilibrium with the environment and, upon restoring equilibrium, spontaneously emits a photon with a wavelength shifted relative to the absorbed photon. Such processes can lead to both heating (Stokes luminescence) and anti-Stokes fluorescence (ASF) cooling. Therefore, it is reasonable to search for active media for RB lasers among RE-doped materials with high ASF cooling efficiency and minimal heat generation during pumping and stimulated emission in the region of wavelengths under consideration.

In [1–3], a scheme is constructed for theoretically evaluating parameters of solid-state RB lasers. References [4,5] provide analytical expressions for minimum pump power, RB generation efficiency, and maximum signal gain. References [6,7] explore strategies to minimize waste heat through anti-Stokes fluorescence cooling. A proposed method offers substantial reductions in heat generation within controlled laser systems. Reference [8] offers a comprehensive review of both experimental and theoretical advancements in radiation-balanced bulk lasers, fiber lasers, disk lasers, and micro-lasers.

Among the active media for RB lasers and optical cooling, materials doped with RE ions hold a special significance, as discussed in [9–19]. Notably, due to the favorable spectroscopic properties of the ytterbium ion (high absorption coefficient, absence of up-conversion transitions, and low multi-phonon nonradiative processes), initial focus was

directed towards Yb^{3+}-doped materials [2,9–17]. The first athermal bulk laser using direct diode pumping was experimentally demonstrated with a Yb^{3+}:$KGd(WO_4)_2$ crystal [13]. It is noteworthy that, due to the characteristic structure of the absorption and emission spectra of the Yb^{3+} ion, the RB generation wavelength is constrained to the range of 990–1130 nm [4]. Therefore, the search for new doped materials and RB generation channels involving other rare-earth ions is of particular interest. In [18], the RB laser capabilities of a $LiNbO_3$:Tm^{3+} crystal were investigated within the wavelength range of 1650–2000 nm.

Note that, for several reasons (such as the near-unity quantum yield of luminescence and the absence or low efficiency of other excitation relaxation channels), the most popular ion is Yb^{3+}. Consequently, research is primarily focused on Yb^{3+}-doped materials. For other rare-earth (RE) ions, only transitions between the ground and first excited manifolds are considered, which limits the range of generation wavelengths.

This paper valuates the RB generating capabilities of the crystal LN:Ho in the 640–670 nm spectral region corresponding to transitions between the Stark sublevels of the $^5F_5$ and $^5I_8$ manifolds.

2. Materials and Methods

High-purity compounds from Johnson-Mattey (Oberhausen, Germany) (Nb_2O_5, 99.995%) and Merck (Darmstadt Germany) (Li_2CO_3, 99.995%) in powder form were used as the starting materials for the sintering of congruent-composition LN charges. Ho ions of high purity with a concentration of 1at% and the form of holmium oxide (Ho_2O_3, 99.99%) from Merck were added to the initial melt. Crystals were grown by a modified Czochralski method in air atmosphere with a platinum crucible with dimensions of $40 \times 40 \times 2$ mm^3. A radio-frequency heating furnace was utilized, heating the crucible and after-heater. Crystals were pulled along the c axis of the LN crystal with a speed of 2 mm/h and rotation rate of 20 rpm. During the growth process, an electric field was applied to the crystal–melt system with a dc electric current of around 12 A/m. The latter provides the possibility to obtain single-domain crystals directly during the growth process and contributes to a high homogeneity of the crystals [19]. Obtained crystals were orientated along the crystallographic axis, cut to $10 \times 4 \times 8$ mm^3 (X × Y × Z) size samples, and then handled and polished.

The absorbance of the crystal LN doped with 1.0at% Ho^{3+} ions was carried out at room temperature using a Varian Cary 500 Scan UV-Vis NIR Spectrophotometer (Markham, Canada). The emission cross-section was determined by the reciprocity method using the measured absorption cross-section.

As is known, for RB generation to occur, condition (1) must be fulfilled [1]

$$\lambda_f < \lambda_p < \lambda_L \tag{1}$$

where λ_p and λ_L are the pump and generation wavelengths, respectively, and λ_f is the average luminescence wavelength, defined as

$$\lambda_f = \frac{\int \lambda I_{em}(\lambda) d\lambda}{\int I_{em}(\lambda) d\lambda} \tag{2}$$

$I_{em}(\lambda)$—spectral dependence of the emission intensity.

The efficiencies of RB generation and maximum signal amplification at high pumping intensities, as well as the efficiency per unit length of the optical cooling process, are defined as follows [4,5]:

$$\eta_L(\lambda_p, \lambda_L, I_p) \equiv \frac{1}{I_p}\frac{\partial I_L}{\partial z} = \sigma_{abs}(\lambda_p) N_t \eta_o \frac{\beta(\lambda_p) - \beta(\lambda_L)}{\beta(\lambda_p)} \tag{3}$$

$$g_{max} = \sigma_{abs}(\lambda_L) N_t \frac{\beta(\lambda_p) - \beta(\lambda_L)}{\beta(\lambda_L)} \tag{4}$$

$$F_{cool} = \sigma_{abs}(\lambda_p)\left[\frac{\lambda_p}{\lambda_f} - 1\right] \quad (5)$$

(where $\eta_o = \left(\lambda_p - \lambda_f\right)/\left(\lambda_L - \lambda_f\right)$) is the intrinsic optical efficiency of the continuous RB laser, and N_t is the concentration of impurity ions,

$$\beta(\lambda) = \frac{\sigma_{abs}(\lambda)}{\sigma_{abs}(\lambda) + \sigma_{em}(\lambda)} \quad (6)$$

$\sigma_{abs}(\lambda)$ and $\sigma_{em}(\lambda)$ are the absorption and emission cross-sections.

The condition of radiation balance in the laser, taking into account the contributions of heat released in the pumping and signal amplification processes, is [5,17]

$$1 - \frac{I_L^{min}}{I_L} - \frac{I_p^{min}}{I_p} = 0 \quad (7)$$

where I_p and I_L are the pump and laser intensities,

$$I_k^{min} = \frac{1}{\beta(\lambda_k)} \times \frac{\beta(\lambda_p)\beta(\lambda_L)}{\beta(\lambda_p) - \beta(\lambda_L)} \times \frac{\lambda_L}{\lambda_f}\left(\frac{\lambda_p - \lambda_f}{\lambda_L - \lambda_p}\right) I_{sat,\,k} \quad k = p,\ L \quad (8)$$

Pump saturation intensity ($k = p$) and emission ($k = L$) are determined by the expression [17]

$$I_{sat,\,k} = \frac{hc}{\lambda_k \tau_r (\sigma_a(\lambda_k) + \sigma_{em}(\lambda_k))} \quad (9)$$

where τ_r is the radiation lifetime of the excited multiplet, h is Planck's constant, and c is the speed of light.

From (7), it follows that as the pump intensity becomes larger ($I_p \to \infty$), the signal intensity asymptotically approaches a constant value $I_L = I_L^{min}$. The same is also true for the pump intensity, meaning that if $I_L \to \infty$, then $I_p = I_p^{min}$.

Note that the dependence imposed by the radiation balance condition on the pump and radiation intensities differs significantly from the dependence in a typical laser, for which the pump and signal have a linear dependence, $I_L \sim I_P$.

3. Results

The absorption spectrum is shown in Figure 1(I), from which the absorption cross-section is determined; $\sigma_{abs}(\lambda) = k(\lambda)/N_{Ho}$ ($N_{Ho} = 1.67 \times 10^{20}$ cm^{-3} is the concentration (Ho^{3+} ion) (Figure 1(II-a)). Figure 2 shows the energy diagram of the Stark levels of the ground, $^5I_8$, and excited, $^5F_5$, manifolds of the Ho^{3+} ion in the LN crystal [20].

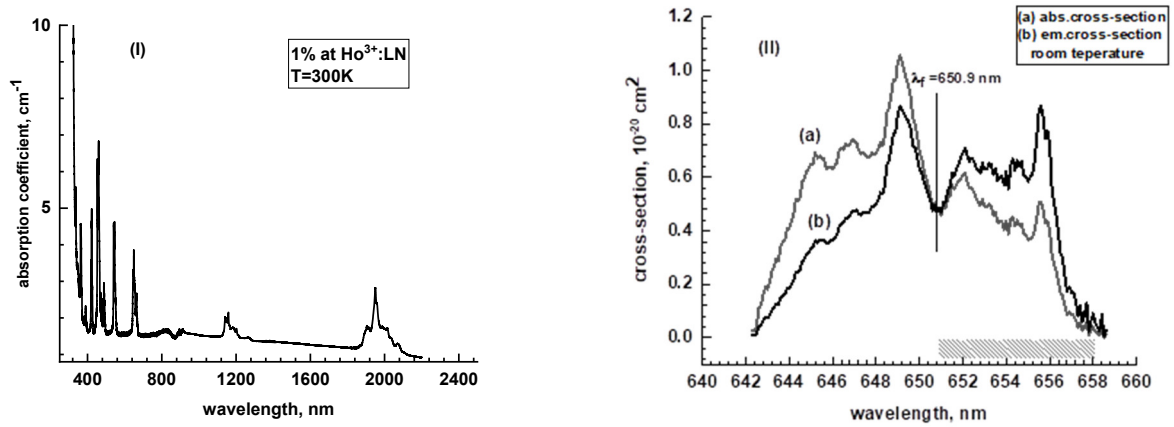

Figure 1. (**I**) Absorption coefficient; (**II**) absorption (a) and emission (b) cross-sections of LN:1at%Ho.

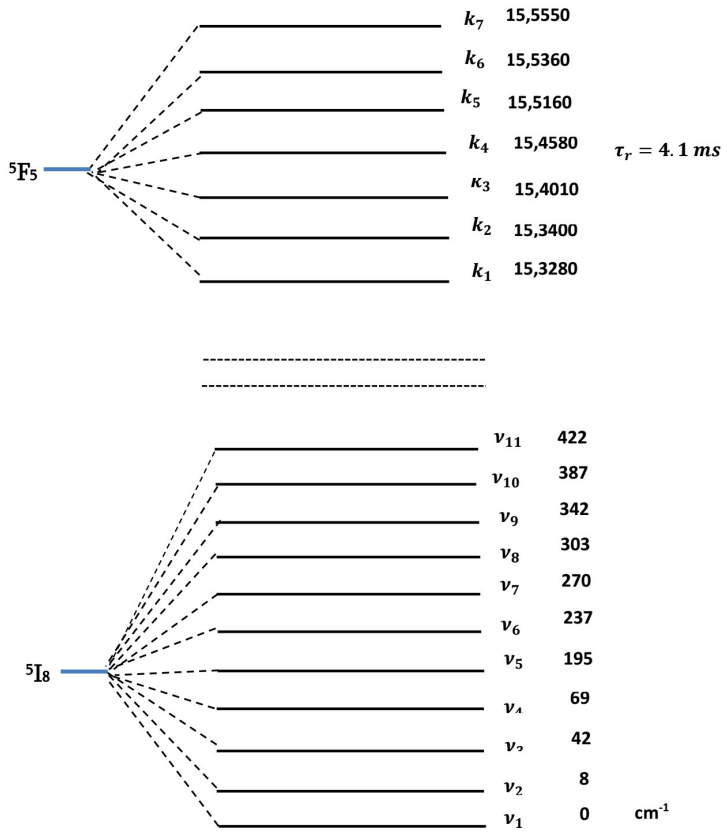

Figure 2. Energies of Stark levels of LN:Ho [21].

Note that if the energy levels of the upper and lower manifolds are known, then, according to the principle of reciprocity, the absorption and emission cross-sections are related by the following relation [5,22]:

$$\sigma_{em}(\lambda) = \sigma_{abs}(\lambda)\frac{Z_{gr}}{Z_{up}}\ exp\left(\frac{E_0 - \frac{hc}{\lambda}}{kT}\right) \tag{10}$$

where E_o is the energy distance between the lower sublevels of the ground and upper manifolds, $Z_{gr,\,up} = \sum_i g_i exp\left[\left(E_1^{(gr,up)} - E_i^{(gr,up)}\right)/k_B T\right]$ is the statistical weights of the ground and upper manifolds ($E_i^{(gr,up)}$ and g_i are the energy and degeneration of the ith sublevel of the ground and upper manifolds), k_B is the Boltzmann constant, and T is the temperature. Relation (10) allows us to express the main characteristics of RB lasing through the parameters E_0, $\sigma_{abs}(\lambda)$, Z_{gr}, and Z_{up}. Indeed, substituting (10) into (6), and (3) and (4), we obtain the following:

$$\beta(\lambda) = \left[1 + \frac{Z_{gr}}{Z_{up}} exp\left(\frac{E_0 - hc/\lambda}{kT}\right)\right]^{-1} \tag{11}$$

$$\eta_L(\lambda_p, \lambda_L, I_p) = \frac{Z_{gr}}{Z_{up}}\eta_0 N_t \sigma_{abs}(\lambda_P) exp\left(\frac{E_0}{kT}\right)\left[exp\left(\frac{-hc/\lambda_L}{kT}\right) - exp\left(\frac{-hc/\lambda_p}{kT}\right)\right]\beta(\lambda_L) \tag{12}$$

$$g_{max} = \frac{Z_{gr}}{Z_{up}} N_t \sigma_{abs}(\lambda_L) exp\left(\frac{E_0}{kT}\right)\left[exp\left(\frac{-hc/\lambda_L}{kT}\right) - exp\left(\frac{-hc/\lambda_p}{kT}\right)\right]\beta(\lambda_p) \tag{13}$$

The use of expressions (11), (12), and (13) significantly simplifies both the qualitative analysis of the capabilities of specific materials doped with rare-earth elements for RB generation and the procedure of quantitative calculations.

Using the calculated values of the statistical weights of $^5I_8$ and $^5F_5$ manifolds (Z_{gr} = 8.0606 and Z_{up} = 6.7192), the emission cross-section in the wavelength range 640–670 nm was determined by Formula (10) (Figure 1(II-b)). Noting that $I_{em}(\lambda) \sim \lambda^5\sigma_{em}(\lambda)$,, for the average fluorescence wavelength calculated by the formula $\lambda_f = \int \left(\sigma_{em}(\lambda)/\lambda^4\right)d\lambda / \int \left(\sigma_{em}(\lambda)/\lambda^5\right)d\lambda$, we obtain $\lambda_f = 649.2$ nm.

4. Discussion

Note that Formula (8) is obtained for the case when the luminescence quantum yield (external quantum efficiency) is close to unity ($\eta_{ext} \cong 1$) [1]. Otherwise, the average fluorescence wavelength, λ_f, should be replaced by $\lambda_f^* = \eta_{ext}\lambda_f$. In the case that transitions with $^5F_5$ are under consideration, according to the data presented in [23], $\eta_{ext} \cong 0.54$.

The absorption and emission cross-section spectra and the value of the mean fluorescence wavelength are shown in Figure 1(II). Taking into account condition (1), we choose the following pump wavelengths: 651.5 nm ($\nu_3 \rightarrow k_3$, $\nu_5 \rightarrow k_6$, k_7) and 652.1 nm ($\nu_1, \nu_2 \rightarrow k_1, k_2$; $\nu_4 \rightarrow k_3$, $\nu_6 \rightarrow k_7$), corresponding to the maxima of the ASF cooling efficiency (5). According to (1), RB generation can occur at the following wavelengths: 653.2 nm ($k_2 \rightarrow \nu_3$, $k_6 \rightarrow \nu_6$), 654.5 nm ($k_2 \rightarrow \nu_3$, $k_2 \rightarrow \nu_4$, $k_5 \rightarrow \nu_6$), 655.9, and 655.6 nm ($k_1 \rightarrow \nu_4$, $k_4 \rightarrow \nu_5$, $k_6 \rightarrow \nu_7$, $k_7 \rightarrow \nu_8$, $k_3 \rightarrow \nu_6$, $k_5 \rightarrow \nu_7$), corresponding to the maxima of the emission spectrum (Figure 1(II-b)). The transitions corresponding to the wavelengths of spectral lines with linewidth accuracy ($\Delta\lambda \approx 0.5$ nm) are given in the brackets. Using the value of the radiative lifetime of the level $^5F_5$, $\tau_r = 0.62$ ms can be calculated by the formula obtained by transformation of the Fuchtbauer–Ladenburg formula [21],

$$\frac{1}{\tau_r} = 8\pi c n^2 \int \frac{\sigma_{em}(\lambda)}{\lambda^4} d\lambda \quad (14)$$

Here, n = 2.287—refractive index at the considered wavelengths [24]); the calculated RB generation efficiency parameters are as follows: $F_{eff} = \eta\left(\lambda_p, \lambda_L, I_p\right)/N_t$, $F_{gain} = g_{max}/N_t$ (Table 1).

Table 1. Parameters characterizing the RB lasing of LN:Ho in 640–670 nm regions.

λ_p, nm	F_{cool}, 10^{-22}cm^2	λ_L, nm	η_0, %	$I_{p_{min}}$	$I_{L_{min}}$	F_{eff}	F_{gain}
				kW/cm^2		10^{-22}cm^2	
651.5	0.03	653.2	26.1	170.4	50.90	0.76	2.12
		654.5	16.7	154.9	17.23	0.85	2.27
		655.6	12.8	101.58	13.89	0.88	8.22
		655.9	12.0	47.33	7.43	2.71	7.08
652.1	0.114	654.5	33.3	111.88	52.43	1.63	7.29
		655.6	25.5	64.47	43.11	3.23	6.08
		655.9	24.0	57.18	74.03	3.29	3.26

It can be seen that the optimal pump and emission wavelengths maximizing the product of $\eta \times g_{max}$ are λ_{OP} = 652.1 nm and λ_{OL} = 655.6 nm. At the same time, RB generation at a wavelength of 655.9 nm, with sufficiently high efficiency, can also occur with pumping at a wavelength of 651.5 nm (Table 1).

A graph of the dependence of the emission intensity on the pump intensity (Equation (7)) at wavelengths of 652.1 nm and 651.5 nm, at which the radiation balance at RB lasing at wavelengths of 655.6 nm and 655.9 nm, respectively, is shown in Figure 3.

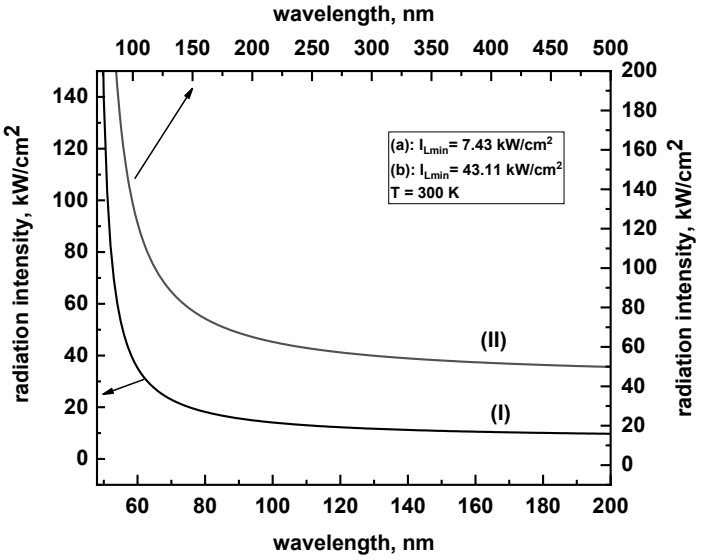

Figure 3. Dependence of RB lasing intensity versus pumping intensity: (I) $\lambda_p = 651.5$ nm and $\lambda_L = 655.9$ nm; (II) $\lambda_p = 652.1$ nm and $\lambda_L = 655.6$ nm.

For comparison, Table 2 shows the values of the RB generation parameters of materials doped with RE^{3+}. It is evident that the unconditional leader is the $KY(WO_4)_2$:Yb^{3+} crystal, whose quality factor for both optical cooling and RB generation ($\lambda_{oL} = 1041$ nm) is an order of magnitude higher than that of other materials. At the same time, it is clear that the RB generation capabilities of this crystal are not only on par with but in many ways exceed the generation capabilities of many other materials, which may incentivize further theoretical and experimental research.

Table 2. Parameters of optimal RB generation of RE^{3+}-doped materials.

Matrix	λ_F	λ_{op}	λ_{OL}	η_o	τ	$I_{P_{min}}$	$I_{L_{min}}$	F_{cool}	F_{eff}	F_{gain}
	nm			%	mc	kW/cm^2			10^{-22} cm^2	
LN:Ho current article	650.1	652.1	655.6	25.5	0.6	64.5	43.1	0.11	3.23	6.08
LN:Tm [18]	1818.6	1919	1929	90	1.1	45.9	93.0	0.10	0.80	0.81
YAG:Yb ceramics [11]	1018	1030	1050	39	0.9	5.9	53.3	0.14	3.3	1.3
LuAG:Yb [2]	1002	1033	1048	67	0.9	26	303	0.49	5.1	0.8
$KY(WO_4)_2$:Yb [5]	992	1002	1041	20	0.6	1.6	5.5	1.50	41	36
ZBLANP:Yb [25]	995	1005	1024	36	1.7	38	46	0.07	1.3	2.4
Rb_2NaYF_6:Yb [26]	996	1011	1068	20	10.8	1.8	17	0.02	0.25	0.34

5. Conclusions

Holmium-doped congruent-composition lithium niobate crystals were grown by the Czochralski method. The absorption of the LN:1at% Ho^{3+} crystal was measured at room temperature. On the basis of the analysis of emission and absorption spectra of the crystal LN:Ho, the possibilities of obtaining, at room temperature, RB lasing in the spectral region 640–670 nm, corresponding to the inter-Stark transition $^5F_5$ and $^5I_8$ multiplets, were investigated. The RB lasing parameters were calculated and the optimal pump and laser wavelengths were determined: $\lambda_{OP} = 652.1$ nm and $\lambda_{OL} = 655.6$ nm. At the same time, the efficiency of RB lasing and radiation amplification ($F_{eff} = 3.23 \times 10^{-22}$ cm^2, $F_{gain} = 6.08 \times 10^{-22}$ cm^2) is high enough. Note that RB generation at a wavelength of 655.9 nm with a sufficiently high efficiency (Table 1) can also occur with pumping at a wavelength of 652.1 nm. However, the minimum values of pumping and generation intensities are rather high (Table 1), which is likely to complicate experimental studies of RB laser capabilities in the wavelength region under consideration.

From the data presented in Table 2, it is evident that the RB generation capabilities of the LN:Ho crystal are highly competitive and surpass those of many other materials. This may incentivize further theoretical and experimental research.

Author Contributions: Conceptualization, G.D. and E.K.; methodology, G.D.; software, N.B.; validation, E.K. and M.B.; investigation, N.K., M.B. and E.K.; data curation, N.K. and N.B.; writing—original draft preparation, E.K. and G.D.; writing—review and editing, E.K. and G.D.; visualization, F.V. All authors have read and agreed to the published version of the manuscript.

Funding: The research was supported by the Higher Education and Science Committee of MESCS RA (Re-search project No. 21T-1C275).

Data Availability Statement: Data is contained within the article.

Conflicts of Interest: The authors declare no conflict of interest.

References

1. Bowman, S. Lasers without internal heat generation. *IEEE J. Quantum Electron.* **1999**, *35*, 115–122. [CrossRef]
2. Mungan, C.E.; Gosnell, T.R. Laser Cooling of Solids. *Adv. At. Mol. Opt. Phys.* **1999**, *40*, 161–228.
3. Mungan, C.E. Radiation thermodynamics with applications to lasing and fluorescent cooling. *Am. J. Phys.* **2005**, *73*, 315–322. [CrossRef]
4. Bowman, S.; Mungan, C. New materials for optical cooling. *Appl. Phys. B Laser Opt.* **2000**, *71*, 807–811. [CrossRef]
5. Bowman, S.R.; Mungan, C.E. Selecting materials for radiation balanced lasers. In *Advanced Solid-State Lasers*; Trends in Optics and Photonics; Injeyan, H., Keller, U., Marshall, C., Eds.; Optical Society of America: Washington, DC, USA, 2000; Volume 34, pp. 446–453.
6. Bowman, S.R.; O'Connor, S.P.; Biswal, S.; Condon, N.J.; Rosenberg, A. Minimizing Heat Generation in Solid-State Lasers. *IEEE J. Quantum Electron.* **2010**, *46*, 1076–1085. [CrossRef]
7. Bowman, S.R. Optically cooled lasers. In *Laser Cooling: Fundamental Properties and Application*; Nemova, G., Ed.; Pan Stanford Publishing Pte. Ltd.: Singapore, 2016; pp. 147–180.
8. Nemova, G. Radiation-Balanced Lasers: History, Status, Potential. *Appl. Sci.* **2021**, *11*, 7539. [CrossRef]
9. Yang, Z.; Meng, J.; Albrecht, A.R.; Sheik-Bahae, M. Radiation-balanced Yb:YAG disk laser. *Opt. Express* **2019**, *27*, 1392–1400. [CrossRef] [PubMed]
10. Bowman, S.R.; O'Connor, S.; Biswal, S. Ytterbium laser with reduced thermal heating. *IEEE J. Quantum Electron.* **2005**, *41*, 1510–1517. [CrossRef]
11. Demirkhanyan, G.; Patrizi, B.; Toci, G.; Vannini, M.; Pirri, A.; Li, J.; Feng, Y.; Zargaryan, D.; Kostanyan, R. YAG-Yb Ceramics as a Material for Radiation Balanced Lasing. *J. Contemp. Phys.* **2022**, *57*, 123–126. [CrossRef]
12. Cheng, L.; Andre, L.B.; Rytz, D.; Rand, S.C. Radiation-balanced lasing in Yb^{3+}:YAG and Yb^{3+}:KYW. *Optics Express* **2023**, *31*, 11994–12004. [CrossRef]
13. Bowman, S.R.; Jenkins, N.; Feldman, B.; O'Connor, S. Demonstration of a radiatively cooled laser. In Proceedings of the Conference on Lasers and Electro-Optics (CLEO), Long Beach, CA, USA, 19–24 May 2002; pp. 32–39.
14. DeLoach, L.D.; Payne, S.A.; Kway, W.L.; Tassano, J.B.; Dixit, S.N.; Krupke, W.F. Vibrational structure in the emission spectra of Yb^{3+}-doped apatite crystals. *J. Lumin.* **1994**, *62*, 85–94. [CrossRef]
15. Bruesselbach, H.W.; Sumida, D.S.; Reeder, R.A.; Byren, R.W. Low-heat high-power scaling using InGaAs-diode-pumped Yb:YAG lasers. *IEEE J. Sel. Top. Quantum Electron.* **1997**, *3*, 105–116. [CrossRef]
16. Peysokhan, M.; Mobini, E.; Allahverdi, A.; Abaie, B.; Mafi, A. Characterization of Yb-doped ZBLAN fiber as a platform for radiation-balanced lasers. *Photon-Res.* **2020**, *8*, 202–210. [CrossRef]
17. Mobini Souchelmaei, E. Radiation-Balanced Fiber Lasers and Amplifiers. Ph.D. Thesis, The University of New Mexico, Albuquerque, NM, USA, 2020; 154p.
18. Mkhitaryan, N.; Demirkhanyan, G.; Kokanyan, N.; Kokanyan, E. $LiNbO_3$:Tm^{3+} Crystal: Material for Radiation-Balanced Laser in the Wavelength Range of 1650–2000 nm. *Arm. J. Phys.* **2023**, *16*, 102–108. [CrossRef]
19. Balasanyan, R.N.; Gabrielyan, V.T.; Kokanyan, E.P.; Feldvari, I. Composition and homogeneity of $LiNbO_3$ crystals as re-lated to growth-conditions. 1. The influence of electric-field. *Kristallografiya* **1990**, *35*, 1540–1544.
20. Lorenzo, A.; Bausa, L.E.; Garcia, J.S.; Solé, J.G. Optical absorption intensities and fluorescence dynamics of Ho^{3+} ions in $LiNbO_3$. *J. Phys. Cond. Matter* **1996**, *8*, 5781–5785. [CrossRef]
21. Krupke, W. Induced-emission cross sections in neodymium laser glasses. *IEEE J. Quantum Electron.* **1974**, *10*, 450–457. [CrossRef]
22. Yasyukevich, A.S.; Shcherbitskii, V.G.; Kisel, V.; Mandrik, A.V.; Kuleshov, N.V. Integral method o reciprocity in the spectroscopy of laser crystals with impurity centers. *J. Appl. Spectrosc.* **2004**, *71*, 202–208. [CrossRef]
23. Dai, L.; Jiao, S.; Xu, C.; Qian, Z.; Lin, J.; Xu, Y. Dopant occupancy and optical properties of Ho^{3+} in Hf: Ho: $LiNbO_3$ crystal. *J. Lumin.* **2014**, *150*, 19–24. [CrossRef]
24. Polyanskiy, N. Refractiveindex.info database of optical constants. *Sci. Data* **2024**, *11*, 94. [CrossRef]

25. Hoyt, C.W.; Sheik-Bahae, M.; Epstein, R.I.; Edwards, B.C.; Anderson, J.E. Observation of Anti-Stokes Fluorescence Cooling in Thulium-Doped Glass. *Phys. Rev. Lett.* **2000**, *85*, 3600–3603. [CrossRef] [PubMed]
26. Nemova, G.; Kashyap, R. Laser cooling of solids. *Rep. Prog. Phys.* **2010**, *73*, 086501. [CrossRef]